ARMY RESEARCH LABORATORY

Dynamics of Photo-Excited Carriers and Coherent Effects in GaN Under Subpicosecond Laser Pulse Excitation

by Sergey Rudin, Enrico Bellotti, Gregory A. Garrett, and Michael Wraback

ARL-TR-5403 **November 2010**

NOTICES

Disclaimers

The findings in this report are not to be construed as an official Department of the Army position unless so designated by other authorized documents.

Citation of manufacturer's or trade names does not constitute an official endorsement or approval of the use thereof.

Destroy this report when it is no longer needed. Do not return it to the originator.

Army Research Laboratory
Adelphi, MD 20783-1197

ARL-TR-5403 **November 2010**

Dynamics of Photo-Excited Carriers and Coherent Effects in GaN Under Subpicosecond Laser Pulse Excitation

Sergey Rudin, Gregory A. Garrett, and Michael Wraback
Sensors and Electron Devices Directorate, ARL

Enrico Bellotti
Electrical and Computer Engineering Department, Boston University

REPORT DOCUMENTATION PAGE

Form Approved
OMB No. 0704-0188

1. REPORT DATE *(DD-MM-YYYY)*	2. REPORT TYPE	3. DATES COVERED (From - To)
November 2010		January to October 2010

4. TITLE AND SUBTITLE
Dynamics of Photo-Excited Carriers and Coherent Effects in GaN Under Subpicosecond Laser Pulse Excitation

5a. CONTRACT NUMBER

5b. GRANT NUMBER

5c. PROGRAM ELEMENT NUMBER

6. AUTHOR(S)
Sergey Rudin, Enrico Bellotti, Gregory A. Garrett, and Michael Wraback

5d. PROJECT NUMBER

5e. TASK NUMBER

5f. WORK UNIT NUMBER

7. PERFORMING ORGANIZATION NAME(S) AND ADDRESS(ES)
U.S. Army Research Laboratory
ATTN: RDRL-SEE-M
2800 Powder Mill Road
Adelphi, MD 20783-1197

8. PERFORMING ORGANIZATION REPORT NUMBER
ARL-TR-5403

9. SPONSORING/MONITORING AGENCY NAME(S) AND ADDRESS(ES)

10. SPONSOR/MONITOR'S ACRONYM(S)

11. SPONSOR/MONITOR'S REPORT NUMBER(S)

12. DISTRIBUTION/AVAILABILITY STATEMENT
Approved for public release; distribution unlimited.

13. SUPPLEMENTARY NOTES

14. ABSTRACT
We applied the Semiconductor Bloch Equations formalism to study the subpicosecond dynamics of photo-excited carriers in gallium nitride (GaN). The kinetics equations were derived using a two-band model and taking into account the coherent interaction of semiconductor with the short laser pulse. Various scattering terms due to interaction of carriers with polar optical phonons and carrier-carrier interaction were taken into account. Effects of the conduction band nonparabolicity and static screening were included in our theory. We find reasonable agreement with the experimental results on the time-resolved photoluminescence rise-time dependence on excitation energy and carrier density, thus confirming the dominant role of polar optical phonons in the subpicosecond dynamics, and the effects of screening.

15. SUBJECT TERMS
Photoexcitation, GaN, laser pulses

16. SECURITY CLASSIFICATION OF:			17. LIMITATION OF ABSTRACT	18. NUMBER OF PAGES	19a. NAME OF RESPONSIBLE PERSON
a. REPORT	b. ABSTRACT	c. THIS PAGE	UU	38	Sergey Rudin
Unclassified	Unclassified	Unclassified			19b. TELEPHONE NUMBER (*Include area code*) (301) 394-0206

Contents

List of Figures

Acknowledgment

We thank Anand Sampath for the material growth. We also thank Yang Wang for useful discussions and numerical work in the earlier stages of this project.

INTENTIONALLY LEFT BLANK.

1. Summary

We present a theoretical and experimental study of subpicosecond kinetics of photo-excited carriers in bulk gallium nitride (GaN). The theoretical model uses a simple two-band approximation with the conduction band nonparabolicity taken into account. The scattering mechanisms included in this work are interactions of carriers with polar optical phonons and carrier-carrier Coulomb interaction. Interaction of the semiconductor with the exciting laser pulse is treated coherently, while the scatterings are included in the stochastic Monte Carlo solution of the kinetic equations. The theoretical results are compared with the experimental results of the time-resolved photoluminescence induced by a 100-femtosecond (fs) pulse.

2. Introduction

Ultrafast phenomena in photo-excited semiconductors are of great interest, both theoretically and experimentally. On the experimental side, ultrafast laser technology improved the time resolution of measurements of carrier dynamics. On the time scale of 100 fs, both coherent and non-coherent processes contribute to the observed carrier dynamics. On the theoretical side, there has been much progress toward explaining the experimental results related to dynamics of hot carriers in gallium arsenide (GaAs) and related compounds (*1*). The more traditional approach employs the semi-classical Boltzmann equation that describes the time evolution of carrier density distributions. That equation can be studied by various numerical methods. An especially efficient approach to finding its solutions for given initial conditions is the Monte Carlo simulation (*2*). Because the interband polarization is not included in the Boltzmann transport equations, the coherent effects due to the interaction of the external light field with the semiconductor, and the excitonic effects due to electron-hole interactions, cannot be studied in the semiclassical approximation. For the purpose of modeling various ultrafast phenomena, the density matrix formalism provides a consistent description (*3*). This approach uses perturbation theory to obtain the equations of motion for the distribution functions of hot carriers and for the interband polarization, and takes coherent and dephasing processes into account in a consistent way. The resulting coupled equations are referred to as Semiconductor Bloch Equations (*3*) (SBE), and they replace the Boltzmann transport equation.

In good-quality polar semiconductors, one of the main energy and momentum relaxation mechanisms in carrier kinetics is the interaction of carriers with longitudinal optical (LO) phonons via the Frohlich interaction (*4*). In GaAs, the relaxation rate of electrons at slightly above 1 LO phonon energy is calculated to be about 140 fs (*5*). GaN has larger polarizability, and the electron-phonon emission rates are an order of magnitude higher than in GaAs. In

particular, the relaxation rate of electrons at slightly above 1 LO phonon energy is calculated to be about 12 fs (*6*). Therefore, the carrier dynamics in GaN can be substantially different from dynamics in GaAs. This feature is particularly important in understanding the kinetics of the electron-hole plasma generated by sort laser pulses.

The carrier kinetics study of GaN presented here was motivated by the current interest in application of nitride semiconductors in ultraviolet (UV) optoelectronics, and high temperature and power electronics. The study can be extended to aluminum gallium nitride (AlGaN) compounds. The UV-emitters and UV-detectors in the wavelength region from 300–360 nm and from 250–270 nm will serve as important building blocks of the new generation of biological agent detection systems. GaN is potentially important in many applications, such as power and optoelectronics devices, because it has a number of favorable features, among these a large band gap, high saturation velocity, and high breakdown electric field. A better understanding of hot carrier dynamics can greatly improve the knowledge of the material and design issues, and the performance of devices.

In this work, we use the SBE formalism to study the dynamics of carriers in bulk GaN under subpicosecond laser pulse excitation, and we compare the theoretical results with the experimental results obtained by time-resolved photoluminescence (TRPL) studies (*7*). The kinetic problem we investigate here is illustrated schematically in figure 1.

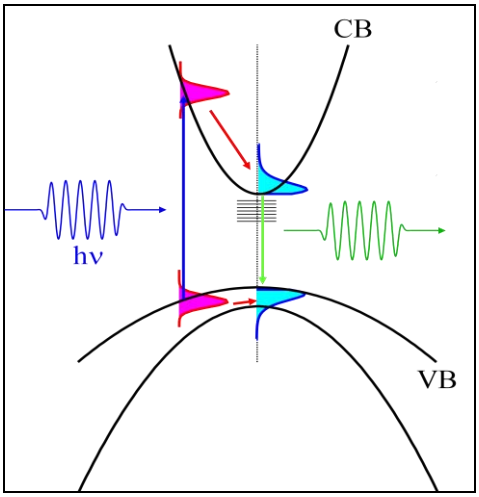

Figure 1. A classical light pulse whose central Fourier component has frequency ν excites electrons and holes in a semiconductor sample. The non-equilibrium distributions of electrons in the conduction band and heavy holes in the valence band undergo intraband relaxation and subsequent interband recombination with light emission. The intraband processes included in this work are carrier-phonon and carrier-carrier scatterings. The effects of the trap states indicated in the figure are not included.

In section 3, we compare single-carrier scattering rates due to various interactions and compare their thermal averages for the equilibrium distributions. We find that with the material

parameters established for the bulk GaN, the intraband relaxation is dominated by the carrier interactions with LO phonons. In section 4, we establish the kinetic equations—the SBE derived from the Heisenberg equations of motion. A simple relaxation time approximation is considered in section 5, where the effects of coherence and dephasing in the interband luminescence are discussed. The theoretical model was developed in conjunction with the experimental studies of the time-resolved spectroscopy of UV luminescence outlined in section 6. The numerical solutions of the SBE were performed using the Monte Carlo method, following the approach of Kuhn and Rossi to account for the effects of the interband polarization (*8, 9*). The results corresponding to lower excitation power are presented in section 7, where they are compared to the available experimental results.

3. Intraband Carrier Scattering Processes

In this work, we use an isotropic two-band model for the Γ valley of conduction electrons with mass $m_e = 0.2m_0$ and heavy holes with mass $m_h = 1.1m_0$, where m_0 is the vacuum electron mass. The nonparabolicity of the conduction band of GaN will be taken into account by analytical approximation similar to the one obtained in Kane's model for a cubic structure (*10*)

$$\frac{\hbar^2 k^2}{2m_e} = E(1+\alpha E) \equiv \gamma(E) \ , \tag{1}$$

where $\alpha = (1 - m_e/m_0)^2(1/E_g)$. The value of the nonparabolicity coefficient α obtained for the wurtzite GaN from full band structure calculations (*11*) turns out to be considerably larger—about 0.37 eV^{-1}. As an approximation here, we will use $\alpha \approx 1/E_g$. The following values will be assumed: $m_e = 0.2m_0$, $m_h = 1.1m_0$, and $E_g = 3.39$ eV.

We assume dispersionless LO phonons with energy $\hbar\omega_{LO} = 91.2$ meV. For the scattering of carriers by LO phonons via the Frohlich interaction, the matrix element in a sample of volume V is

$$M_{FR}^{\alpha}(k,k+q) = \left[\frac{e^2\hbar\omega_{LO}}{q\varepsilon_s\varepsilon_0 V}\left(\frac{1}{\varepsilon_\infty} - \frac{1}{\varepsilon_s}\right)\right]^{1/2} I^{\alpha}(k,k+q) \tag{2}$$

in SI units, where $\varepsilon_s = 5.35$, $\varepsilon_\infty = 8.9$, and the vacuum $\varepsilon_0 = 8.854\times10^{-12}$ F/m. The overlap integrals (*4*) $I(\mathbf{k},\mathbf{k}')$ are given by

$$I^{e}(\mathbf{k},\mathbf{k}') = \frac{(1+\alpha E_k)^{1/2}(1+\alpha E_{k'})^{1/2} + \alpha(E_k E_{k'})^{1/2}\cos\theta_{kk'}}{\left[(1+2\alpha E_k)(1+2\alpha E_{k'})\right]^{1/2}} \tag{3}$$

for the conduction band, and by

$$I^{h}(\mathbf{k},\mathbf{k}') = \frac{1}{2}\left(1+3\cos^{2}\theta_{kk'}\right)^{1/2} \tag{4}$$

for the valence band, where $\theta_{kk'}$ is the angle between the initial and final momenta. The scattering rate is obtained using the Fermi Golden Rule:

$$\Gamma(\mathbf{k}) = (2\pi/\hbar)V\int \frac{d^{3}k'}{(2\pi)^{3}}\left|M(\mathbf{k},\mathbf{k}')\right|^{2}\left[(N_{k-k'}+1)\delta(E_{k}-E_{k'}-\hbar\omega_{LO})+N_{k-k'}\delta(E_{k}-E_{k'}+\hbar\omega_{LO})\right] \tag{5}$$

where N_q is the occupation number of LO phonons, $[\exp(\hbar\omega_{LO}/k_BT) - 1]^{-1}$.

The scattering time defined as $\hbar/\Gamma$ is shown in figure 2 as a function of carrier energy above the band edge for the parabolic case. The corresponding momentum and energy relaxation times (*4*) are also shown.

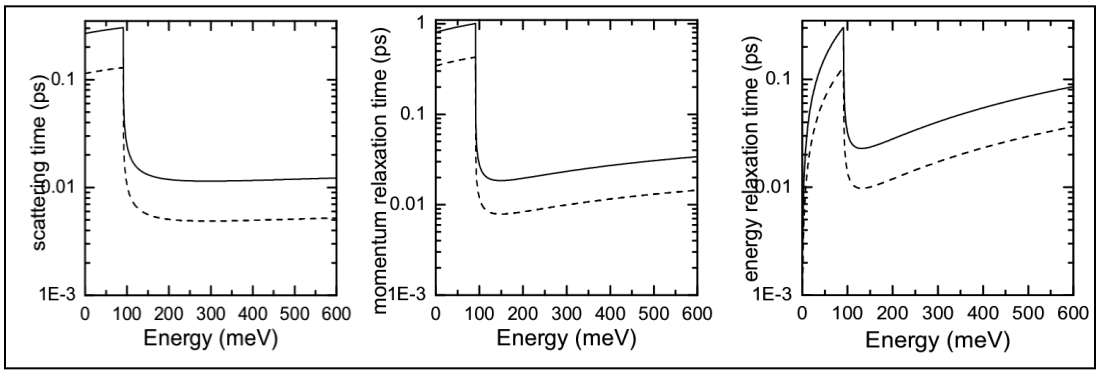

Figure 2. Left panel: scattering times for electron (solid curve) and heavy hole (dashed curve) interacting with polar LO phonons. The corresponding momentum (middle panel) and energy (right panel) relaxation times.

In the presence of other free carriers, the carrier interaction with polar phonons is screened. In the static limit, the screened Frohlich interaction matrix element takes form (*12*)

$$M^{\alpha}_{FR}(\mathbf{k},\mathbf{k}+\mathbf{q}) = \left[\frac{e^{2}\hbar\omega_{LO}}{\varepsilon_{0}V}\left(\frac{1}{\varepsilon_{\infty}}-\frac{1}{\varepsilon_{s}}\right)\right]^{1/2}\frac{q}{q^{2}+\kappa^{2}}I^{\alpha}(\mathbf{k},\mathbf{k}+\mathbf{q}) \ , \tag{6}$$

where the static reciprocal screening length is given by (*3*)

$$\kappa^{2} = -\frac{e^{2}}{\varepsilon_{s}\varepsilon_{0}V}\sum_{k,\alpha}\left(\frac{\partial E_{\alpha}(k)}{\partial k}\right)^{-1}\left(\frac{\partial f^{\alpha}_{k}}{\partial k}\right) \tag{7}$$

in terms of electron and hole distribution functions f^{e} and f^{h}. The effects of nonparabolicity and screening on the electron-LO phonon scattering rates are shown in figures 3 and 4.

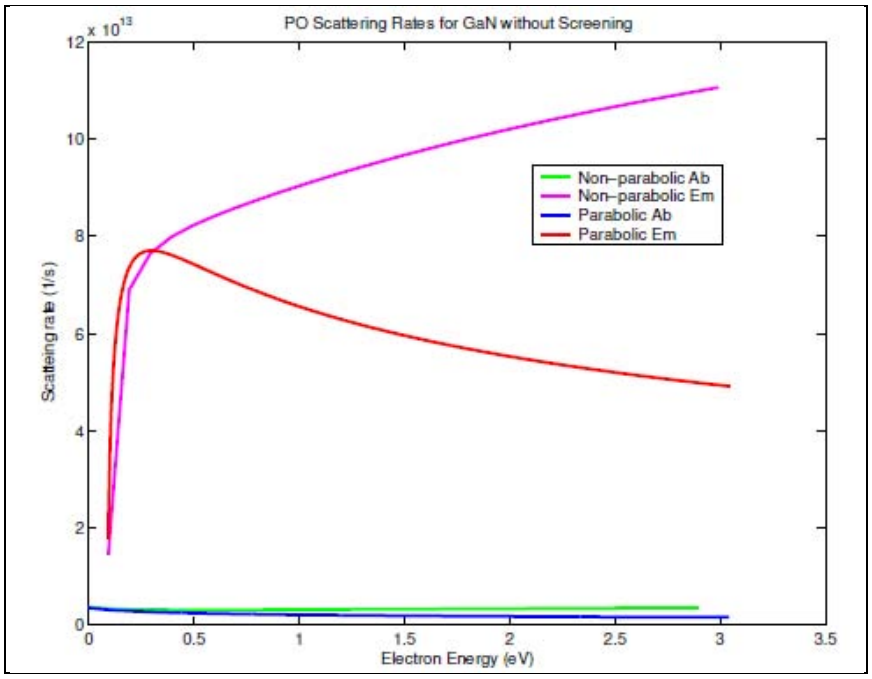

Figure 3. Polar optical phonon scattering rate for non-parabolic band.

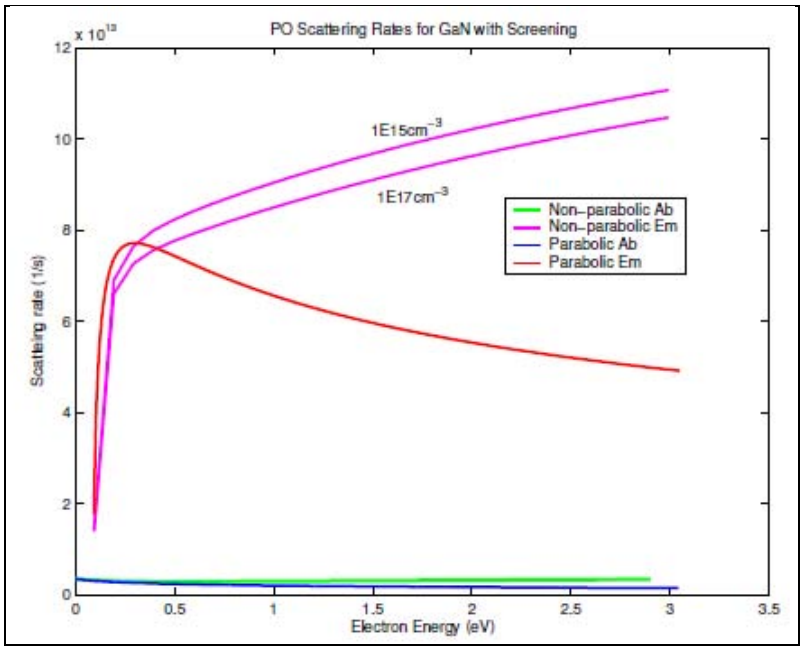

Figure 4. Polar optical phonon scattering rate for non-parabolic band with screening.

The nonparabolicity of the conduction band increases the emission rate of LO phonons for electrons with energy exceeding 0.4 V above the band edge. This is what prevents the runaway hot electron effect in GaN in strong applied field. Both the nonparabolicity and screening will be taken into account later in the numerical simulation of the hot carrier kinetics.

The carrier-carrier scattering proceeds via screened Coulomb interaction:

$$V_q = \frac{e^2}{\varepsilon_0 \varepsilon_s V} \frac{1}{q^2 + \kappa^2}, \tag{8}$$

with the screening wave-vector κ given in equation 7. In the non-degenerate case of carriers with densities n_e and n_h at temperature T, κ becomes the Debye reciprocal screening length defined by $\kappa_0^2 = e^2(n_e+n_h)/\varepsilon_0\varepsilon_s k_B T$, while in the strongly degenerate case it becomes the Thomas-Fermi wave-vector. For the scattering of carriers by ionized impurities, we assume the same screened Coulomb potential as in equation 8, the Brooks-Herring model (*4*).

The criterion for the applicability of classical statistics is the smallness of the thermal wavelength $\lambda = (2\pi\hbar^2/m_e k_B T)^{1/2}$. The electron gas is classical if $\lambda^3 n << 1$, and the quantum statistics are to be used if $\lambda^3 n > 1$. For electrons in GaN at room temperature, we obtain $\lambda^3 n \approx 0.9$ if $n = 10^{18}$ cm^{-3}. Therefore, the electrons become degenerate if $n > 10^{18}$ cm^{-3}.

Consider next the scattering of carriers by acoustic phonons. For the deformation potential interaction the matrix element, assuming a parabolic band and linear phonon dispersion, is given by (*13*)

$$M_{DP}(k,k+q) = D\left[\frac{\hbar q}{2\rho u V}\right]^{1/2}, \tag{9}$$

where D is band deformation potential, ρ is the density, and u is the sound velocity. For GaN ρ = 6.15 g/cm^3, u = 6.56 Km/s, and D = 8.3 eV for the conduction band. For the unscreened piezoelectric interaction

$$M_{PE}(k,k+q) = \frac{e q_l q_j e_{l,ij} \xi_i}{q^2 \varepsilon_0 \varepsilon_s}\left[\frac{\hbar}{2\rho u q V}\right]^{1/2}, \tag{10}$$

where $e_{l,ij}$ is the third rank tensor of the piezoelectric constants, $\boldsymbol{\xi}$ is a unit polarization vector, and summation over repeated indices is implied.

It is generally the case in polar semiconductors that the largest contribution to the electron scattering rate comes from the electron interaction with polar optical phonons (*3, 4*). In order to compare the scattering rates due to different interactions in GaN, let us consider the electron momentum scattering rates (see reference 4 for the definition) and then evaluate their thermal averages for the case of a quasi-equilibrium distribution characterized by electron temperature T_e for the non-degenerate case and a parabolic band. The corresponding momentum relaxation times are shown in figure 5 as functions of electron temperature T_e/T_0 where $T_0 = 300$ K. The electron density was set to $n = 10^{18}$ cm^{-3}, and the impurity density $n_{imp} = 10^{17}$ cm^{-3}.

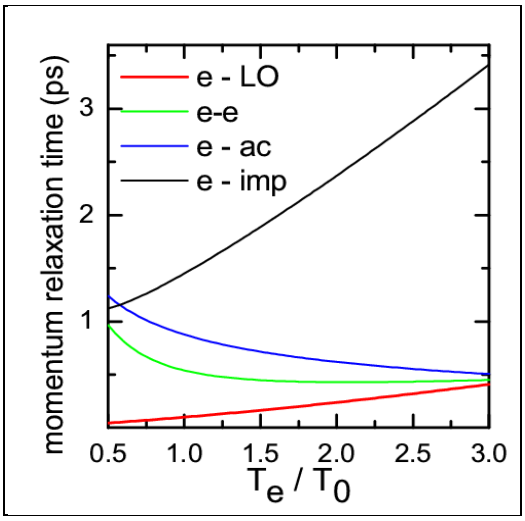

Figure 5. Electron momentum relaxation times obtained from thermally averaged momentum scattering rates, and are shown as functions of electron temperature T_e. The lattice temperature was set to $T_0 = 300$ K, electron density $n = 10^{18}$ cm^{-3}.

From these quasi-equilibrium results, we expect that on the subpicosecond scale the carrier kinetics are dominated by the interactions with polar optical phonons. In the carrier-carrier scattering considered previously, we assumed static screening. When the dynamic screening effects are taken into account, one finds that the electron-hole semiconductor plasma can sustain collective charge density waves, or the plasma oscillations. An electron or a hole whose kinetic energy exceeds a certain threshold value can lose its energy to the collective excitation. The quantum mechanical picture is that of emission of plasmon by a single particle. Alternatively, one can look at the Fermi quasi-particle scattering rate evaluated in the Random Phase Approximation (RPA) and obtain a similar result (*14*). In the long wavelength limit, the frequency for the two component case is obtained as

$$\omega_0^{\,2} = \sum_{\alpha} \frac{e^2 n_\alpha}{\varepsilon_0 \varepsilon_s m_\alpha}\,, \tag{11}$$

in the case of photo-excited electrons and holes $n_e = n_h = n$ and $\omega_0^{\,2} = ne^2/m_r\varepsilon_0\varepsilon_s$, where we defined the reduced mass $m_r = (m_e^{-1} + m_h^{-1})^{-1}$. For GaN, we then obtain

$$\hbar\omega_0 = 30.3 \times \left(\frac{n}{n_0}\right)^{1/2} meV\,. \tag{12}$$

The matrix element for the carrier-plasmon interaction is given by (*15*)

$$M_{\alpha\text{-pl}}(\mathbf{k},\mathbf{k}+\mathbf{q}) = \left[\frac{e^2\hbar^3}{2\varepsilon_0\varepsilon_s m_\alpha^{\,2} V}\right]^{1/2} \frac{2\mathbf{q}\cdot\mathbf{k} + q^2}{2\omega_p(q)q}, \tag{13}$$

where $\omega_p(q)$ is the plasma frequency. Its value at $q = 0$ is given by ω_0. In order to estimate the electron-plasmon scattering rate, we consider a degenerate electron gas characterized by its separate Fermi energy $E_F = (\hbar^2/2m_e)(3\pi^2 n)^{2/3}$, not related to the chemical potential of the equilibrium electron-hole plasma. The plasmon as a well-defined collective excitation is restricted to $q < q_c$, where q_c is the threshold for plasmon decay into the quasi-particle continuum, obtained from the zeroes of the dielectric function in RPA:

$$\frac{q_c k_F \hbar}{m_e} + \frac{q_c^{\,2}\hbar}{2m_e} = \omega_0 \tag{14}$$

If the electron energy, E_k, is much greater than $\hbar\omega_0$, the rate of spontaneous plasmon emission can be approximated (*2*) as

$$\Gamma(k) = \frac{m_e e^2 \omega_0}{4\pi\varepsilon_0\varepsilon_s \hbar^2 k} \ln\left(\frac{\hbar k q_c}{m_e \omega_0}\right), \tag{15}$$

which can be rewritten in terms of electron energy E:

$$\Gamma = \Gamma_0 \left(\frac{n}{n_0}\right)^{1/4} \left(\frac{E_0}{E}\right)^{1/2} \ln\left\{2\left(\frac{E}{E_0}\right)\left[\left(1+\frac{E_F}{E_0}\right)^{1/2} - \left(\frac{E_F}{E_0}\right)^{1/2}\right]\right\}, \tag{16}$$

where $1/\Gamma_0 = \tau_0 \approx 20.5$ fs, $E_0 = \hbar\omega_0$, and $n_0 = 10^{18}$ cm^{-3}. The corresponding scattering time is shown in figure 6 as a function of energy.

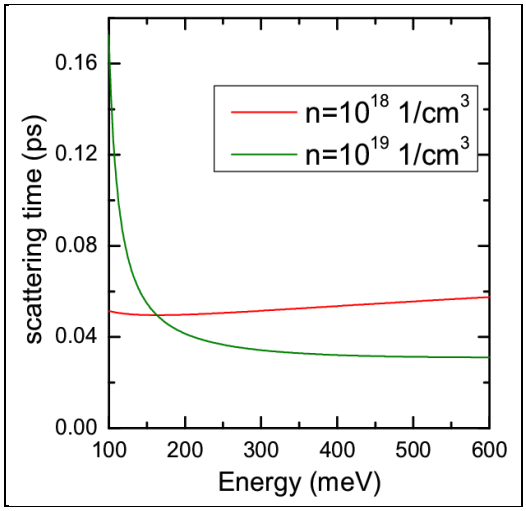

Figure 6. Electron-plasmon scattering time for spontaneous plasmon emission shown as a function of electron energy for two values of density.

We see that the electron-plasmon scattering rate is by a factor of three smaller than the electron-LO phonon rate. In our treatment of SBE, the dynamic screening effects can be accounted for by some of the terms that appear in the second order in carrier-carrier interaction (*1*). We did not include them in this work, but they should be included in the future work.

4. Derivation of Kinetic Equations

The two-band model of carriers (conduction band electrons and valence band holes), interacting with phonons and subjected to a semiclassical electric field, can be defined in terms of creation and annihilation operators for electrons and holes c_k^+, d_k^+,c_k, d_k with Fermi anti-commutation relations, and for phonons, b_k and b_k^+ with Bose commutation relations (*3*). The Hamiltonian of the system is given by $H = H_0 + H_{c\text{-}ph} + H_{c\text{-}c}$, where the first term includes non-interacting carriers in applied field E(t) and unperturbed phonons, the second term describes interaction of carriers with phonons, and the third term describes carrier-carrier interaction. The H_0 is given by

$$\begin{aligned} H_0 &= \sum_k \varepsilon^e(k) c_k^+ c_k + \sum_k \varepsilon^h(k) d_k^+ d_k + \sum_k \hbar\omega(q) b_q^+ b_q \\ &+ \sum_k \left[M_k E(t) e^{-i\omega_p t} c_k^+ d_{-k}^+ + M_k^* E(t) e^{i\omega_p t} d_{-k} c_k \right] \end{aligned} , \tag{17}$$

where $E(t) = E_0 \exp(t^2/\tau_p^2)$ for a Gaussian pulse. The electron and hole energies are given by $\varepsilon^e(k) = E_g + \hbar^2k^2/2m_e$ and $\varepsilon^h(k) = \hbar^2k^2/2m_h$ for parabolic bands, and by equation 1 if the nonparabolicity of the conduction band is included. The optical dipole matrix element in the parabolic bands approximation is given by

$$M_k = d_{cv}\left[1 + \frac{\hbar^2 k^2}{2m_r E_g}\right]^{-1} , \tag{18}$$

which can be approximated by a constant, $M_k \approx d_{cv}$, for large band gap values. The interband electric dipole d_{cv} is related to interband momentum matrix element, $d_{cv}/e = \hbar p_{cv}/E_g m_0$, and in the effective mass approximation for two-band model

$$d_{cv}/e = \left[\frac{-1 + m_0/m_e}{2E_g m_0}\right]^{1/2} , \tag{19}$$

from which we obtain $d_{cv}/e \approx 2.12$ Å.

The carrier-phonon interaction Hamiltonian is given by

$$H_{c-ph} = \sum_{k,q}\left[\gamma^e_{k,k+q} c^+_{k+q} b_q c_k + \gamma^{e*}_{k,k+q} c^+_k b^+_q c_{k+q} + \gamma^h_{k,k+q} d^+_{k+q} b_q d_k + \gamma^{h*}_{k,k+q} d^+_k b^+_q d_{k+q}\right], \tag{20}$$

where for interaction with polar optical phonons the interaction matrix element $\gamma^{e}_{k,k+q} = -\gamma^{h}_{k,k+q} = M_{FR}(k,k+q)$ is given in equation 6, and

$$H_{c-c} = \sum_{k,p,q} V_q \left[\frac{1}{2} c_k^+ c_p^+ c_{p+q} c_{k-q} + \frac{1}{2} d_k^+ d_p^+ d_{p+q} d_{k-q} - c_k^+ d_{-p}^+ d_{-p+q} c_{k-q} \right], \tag{21}$$

where V_q is given in equation 8.

The kinetic variables are the distribution functions of carriers and phonons $f_{\mathbf{k}}^{\alpha}$ and $N_{\mathbf{q}}$, and the interband polarization $p_{\mathbf{k}}$:

$$f_k^e(t) = \left\langle c_k^+(t) c_k(t) \right\rangle \quad f_k^h(t) = \left\langle d_k^+(t) d_k(t) \right\rangle \quad p_k(t) = \left\langle d_{-k}(t) c_k(t) \right\rangle \quad N_q = \left\langle b_q^+ b_q \right\rangle, \tag{22}$$

where all the operators are in Heisenberg representation, and the expectation values are taken with respect to initial state of the system, which is the vacuum of electron-hole pairs and a thermal phonon distribution. The kinetic equations, the SBE, can be derived using the equation of motion for a quantum operator $O_H(t)$ in Heisenberg representation, $i\hbar\partial_t O_H = [O_H, H]$.

4.1 Single-particle Problem

The evolution equations of non-interacting carriers under the action of Hamiltonian H_0 describe the generation of electron-hole pairs in a homogeneous bulk semiconductor by the action of a homogeneous electric field:

$$\left.\frac{df_k^e}{dt}\right|^{(0)} = \left.\frac{df_{-k}^h}{dt}\right|^{(0)} = g_k^{(0)}(t) \tag{23}$$

$$\left.\frac{dp_k}{dt}\right|^{(0)} = \frac{1}{i\hbar}\left[\left(\varepsilon^e(k) + \varepsilon^h(-k) \right) p_k + M_k E_0(t) e^{-i\omega_P t} \left(1 - f_k^e - f_{-k}^h \right) \right] \tag{24}$$

with the generation rate

$$g_k^{(0)}(t) = \frac{1}{i\hbar}\left[M_k E(t) e^{-i\omega_P t} p_k^* - M_k^* E(t) e^{i\omega_P t} p_k \right] \quad . \tag{25}$$

These equations describe a set of independent two-level systems driven by an external field, with a variable detuning Δ_k between the transition energy and the light central frequency,

$$\hbar\Delta_k = \varepsilon^e(k) + \varepsilon^h(k) - \hbar\omega_P \quad . \tag{26}$$

The dynamics at this zero-order approximation are fully coherent. The corresponding Rabi frequency (*3*) is

$$\Omega_R^{(0)} \equiv \frac{d_{cv} E_0}{\hbar} \quad . \tag{27}$$

When the carrier-carrier interactions are taken into account, this value of the Rabi frequency will be changed (renormalized) by the Hartree-Fock terms (*3*). The intensity of the pulse is proportional to $|E(t)|^2$; therefore, if the width of the intensity is τ_w = 100 ft, the corresponding field pulse widths is τ_p = 85 fs. The electric field $E(t) = Re\ E_0 \exp(i\omega_p t - t^2/\tau_p^2)$, and its Fourier transform is

$$\tilde{E}(\omega) = \frac{\tau_p}{\sqrt{2}} e^{-(\omega-\omega_p)^2\tau_p^2/4} \quad ; \tag{28}$$

the energy width is, therefore, $\delta E = 2\hbar/\tau_p \approx 15$ meV.

We have to relate the field strength to the power of the incident pulse train used in the experiments. The energy flux in a single pulse is $S_0(t) = \varepsilon_0 c E^2(t)$, in SI units. Let us assume that the pulses come at a repetition rate ω_r. Then the resulting energy flux is

$$S_p = \omega_r \int_{-\infty}^{\infty} dt\, S_0(t) = \left(\frac{\pi}{8}\right)^{1/2} \omega_r \tau_p \varepsilon_0 c E_{in,0}{}^2 \left(1 - e^{-\omega_p{}^2\tau_p{}^2/2}\right) \quad . \tag{29}$$

In the experimental work described in section 6, the relevant wavelength λ_p of light is in the range 370 to 250 nm, and the corresponding circular frequency $\omega_p = 2\pi c/\lambda$ is in the range $(5.1 - 7.5)\times 10^{15}$ 1/s. Therefore, we can neglect the exponentially small term in equation 29. Equating the flux to the power per unit area, W/A_s, where A_s is approximately the area of the sample surface where the light is absorbed, we obtain a relation between the electric field amplitude and the power:

$$E_{in,0} = \left[\left(\frac{\pi}{8}\right)^{1/2} \frac{W}{\varepsilon_0 \omega_r \tau_p c A_s}\right]^{1/2} \quad . \tag{30}$$

The repetition rate in the experiments was 250 KHz. Assume that the incident spot area A_s = $100\times 100\ \mu m^2$, then for W = 100 μW the corresponding value of $E_{in,0}d_{cv}$ is 3.565 meV. At normal incidence, the ratio of fields in reflected and incident waves is (n–1)/(n+1), and for GaN the reflectance n = 2.2. Then we obtain that in the transmitted wave, $E_0 = 0.927 E_{in,0}$ and $E_0 d_{cv}$ = 3.304 meV, and the corresponding value of the Rabi frequency in equation 27 is 5.02 THz. At arbitrary values of power W, we obtain the following relation between Rabi frequency and the power of the incident pulses (measured in μW):

$$\Omega_R^{(0)} = 0.502\ \mathrm{THz} \times \sqrt{W/1\,\mu W} \quad . \tag{31}$$

The equation 24 for the polarization with the initial condition, $p_k(-\infty) = 0$, can be recast in the integral form, convenient for the discussion of the semiclassical limit:

$$p_k(t) = -i\Omega_R^{(0)} e^{-i\omega_p t} \int_0^{\infty} d\tau e^{-i\Delta_k \tau} E(t-\tau)\left[1 - f_k^e(t-\tau) - f_{-k}^h(t-\tau)\right] \quad . \tag{32}$$

The semiclassical result is obtained by (1) adiabatic approximation $E(t) \rightarrow E(t)\exp(\eta t)$ with $\eta \rightarrow 0^+$ and (2) Markov approximation, in which we assume that the electric field and the distribution functions in the integrand vary slowly compared to oscillations of the exponential factor. These approximations eliminate (1) the influence of initial correlations and (2) the dynamic memory effects. Then the polarization in equation 32 is an instantaneous function of the carrier distribution and applied field. Using the relation

$$\int_0^\infty d\tau\, e^{-(\eta + i\Delta_k)\tau} = -i\frac{P}{\Delta_k} + \pi\delta(\Delta_k)\,,$$

where *P* denotes the principal value and $\delta(x)$ is the Dirac's delta-function, we obtain the semiclassical generation rate from equation 25 in the form of the Fermi's Golden Rule,

$$g_{\mathbf{k}}^{(0)}(t) = 2\pi\Omega_{\mathbf{R}}^{(0)2}\left|E(t)\right|^2\left[1 - f_{\mathbf{k}}^{e}(t) - f_{-\mathbf{k}}^{h}\right]\delta(\Delta_{\mathbf{k}}) \quad . \tag{33}$$

If the Markov approximation in equation 32 is applied to the carrier distribution functions and we retain the time dependence of the Gaussian field, we obtain the effects of the non-zero spectral width of the pulse:

$$g_k^{(0)}(t) = 2\Omega_R^{(0)2}\tau_p e^{-t^2/\tau_p^2}\left[1 - f_k^e(t-\tau) - f_{-k}^h(t-\tau)\right]\int_0^\infty du\cos\left(\Delta_k\tau_p u\right)e^{-(u - t/\tau_p)^2}\,. \tag{34}$$

For times shorter than $\Delta_k\tau_p^2$, the semiclassical generation rate can be approximately factorized into the temporal and spectral pulse shapes (*1*):

$$g_k^{(0)}(t) = 2\Omega_R^{(0)2}\tau_p\left[1 - f_k^e(t-\tau) - f_{-k}^h(t-\tau)\right]e^{-t^2/\tau_p^2}e^{-\Delta_k^2\tau_p^2/4}. \tag{35}$$

4.2 Carrier-phonon Interaction

The contributions of carrier-phonon interaction are obtained by evaluation of the commutation of carrier operators in equation 22 with $H_{c\text{-}ph}$ in equation 20. The resulting contribution to the equation for the electron distribution function is given by

$$\left.\frac{df_k^e}{dt}\right|_{c\text{-}ph} = \frac{1}{i\hbar}\sum_q\left[\gamma_q^e\left\langle c_k^+ b_q c_{k-q}\right\rangle - \gamma_q^e\left\langle c_{k+q}^+ b_q c_k\right\rangle + \gamma_q^{h\,*}\left\langle c_k^+ b_q^+ c_{k+q}\right\rangle - \gamma_q^{h\,*}\left\langle c_{k-q}^+ b_q^+ c_k\right\rangle\right] \tag{36}$$

and similarly for f^h_k and p_k. The lowest order approximation, the first order contribution, is obtained by factorizing the expectation values of three-operator products into distribution functions and polarization. The resulting first-order contributions vanish because $\left\langle b_q\right\rangle = \left\langle b_q^+\right\rangle = 0$ for the eigen-states of the phonon number operator, and, consequently, also in the averaging with the thermal phonons density matrix. In order to obtain the second-order contribution, we have to derive equations of motion for the three-operator products on the right hand side of equation 36.

Again, using commutation and anti-commutation relations in the Heisenberg equation of motion for the operator products, we obtain

$$\begin{aligned}\frac{\mathrm{d}}{\mathrm{dt}}\left\langle \mathrm{c}_{\mathrm{k}}^{+}\mathrm{b}_{\mathrm{q}}\mathrm{c}_{\mathrm{k-q}}\right\rangle &= \frac{1}{\mathrm{i}\hbar}\left[-\varepsilon^{\mathrm{e}}(\mathrm{k})+\varepsilon^{\mathrm{e}}(\mathrm{k}-\mathrm{q})+\hbar\omega(\mathrm{q})\right]\left\langle \mathrm{c}_{\mathrm{k}}^{+}\mathrm{b}_{\mathrm{q}}\mathrm{c}_{\mathrm{k-q}}\right\rangle \\ &+\frac{1}{\mathrm{i}\hbar}\sum_{\mathrm{q}'}\left[\gamma_{\mathrm{q}}^{\mathrm{e}}\left(\left\langle \mathrm{c}_{\mathrm{k}}^{+}\mathrm{b}_{\mathrm{q}}\mathrm{b}_{\mathrm{q}'}\mathrm{c}_{\mathrm{k-q-q}'}\right\rangle-\left\langle \mathrm{c}_{\mathrm{k+q}'}^{+}\mathrm{b}_{\mathrm{q}}\mathrm{b}_{\mathrm{q}'}\mathrm{c}_{\mathrm{k-q}}\right\rangle\right)+\gamma_{\mathrm{q}}^{\mathrm{e}*}\left(\left\langle \mathrm{c}_{\mathrm{k}}^{+}\mathrm{b}_{\mathrm{q}}\mathrm{b}_{\mathrm{q}'}^{+}\mathrm{c}_{\mathrm{k-q+q}'}\right\rangle-\left\langle \mathrm{c}_{\mathrm{k-q}'}^{+}\mathrm{b}_{\mathrm{q}'}^{+}\mathrm{b}_{\mathrm{q}}\mathrm{c}_{\mathrm{k-q}}\right\rangle\right)\right] \\ &+\frac{1}{\mathrm{i}\hbar}\sum_{\mathrm{k}'}\left[\gamma_{\mathrm{q}}^{\mathrm{e}}\left\langle \mathrm{c}_{\mathrm{k}}^{+}\mathrm{c}_{\mathrm{k}'}^{+}\mathrm{c}_{\mathrm{k}'+\mathrm{q}}\mathrm{c}_{\mathrm{k-q}}\right\rangle+\gamma_{\mathrm{q}}^{\mathrm{e}*}\left\langle \mathrm{c}_{\mathrm{k}}^{+}\mathrm{d}_{\mathrm{k}'}^{+}\mathrm{d}_{\mathrm{k}'+\mathrm{q}}\mathrm{c}_{\mathrm{k-q}}\right\rangle\right]\end{aligned} \tag{37}$$

,

and similarly for the other terms. The second-order approximation is obtained by factorizing the expectation values of four-operator products into distribution functions of electrons and phonons, and polarization, and neglecting the two-particle correlations. Define

$$S_{q,k,k-q}^{e}=\left\langle \mathrm{c}_{\mathrm{k}}^{+}\mathrm{b}_{\mathrm{q}}\mathrm{c}_{\mathrm{k-q}}\right\rangle \tag{38}$$

and obtain the equation:

$$\begin{aligned}\frac{\mathrm{d}}{\mathrm{dt}}\mathrm{S}_{\mathrm{q,k,k-q}}^{\mathrm{e}} &= \frac{1}{\mathrm{i}\hbar}\left[-\varepsilon^{\mathrm{e}}(\mathrm{k})+\varepsilon^{\mathrm{e}}(\mathrm{k}-\mathrm{q})+\hbar\omega(\mathrm{q})\right]\mathrm{S}_{\mathrm{q,k,k-q}}^{\mathrm{e}}+\frac{1}{\mathrm{i}\hbar}\gamma_{\mathrm{q}}^{\mathrm{e}*}\left[\left(\mathrm{N}_{\mathrm{q}}+1\right)\mathrm{f}_{\mathrm{k}}^{\mathrm{e}}-\mathrm{N}_{\mathrm{q}}\mathrm{f}_{\mathrm{k-q}}^{\mathrm{e}}\right]-\frac{1}{\mathrm{i}\hbar}\gamma_{\mathrm{q}}^{\mathrm{e}}\mathrm{f}_{\mathrm{k}}^{\mathrm{e}}\mathrm{f}_{\mathrm{k-q}}^{\mathrm{e}} \\ &-\frac{1}{\mathrm{i}\hbar}\gamma_{\mathrm{q}}^{\mathrm{e}*}\mathrm{p}_{\mathrm{k}}^{*}\mathrm{p}_{\mathrm{k-q}}\end{aligned} \tag{39}$$

where we used $\left\langle \mathrm{b}_{\mathrm{q}}^{+}\mathrm{b}_{\mathrm{q}}\right\rangle=\mathrm{N}_{\mathrm{q}}$. This equation has the form

$$\frac{\mathrm{d}}{\mathrm{dt}}\mathrm{S}(\mathrm{t})=-\mathrm{i}\omega\mathrm{S}(\mathrm{t})+\mathrm{Y}(\mathrm{t}). \tag{40}$$

With the initial condition giving $S(t_0)$, it can be cast into the integral form

$$\mathrm{S}(\mathrm{t})=\mathrm{S}(\mathrm{t}_0)\mathrm{e}^{-\mathrm{i}\omega(\mathrm{t}-\mathrm{t}_0)}+\int_{0}^{\mathrm{t}-\mathrm{t}_0}\mathrm{d}\tau\mathrm{e}^{-\mathrm{i}\omega\tau}\mathrm{Y}(\mathrm{t}-\tau) \tag{41}$$

We perform the adiabatic approximation by changing $\omega \rightarrow \omega + 0^{+}$ and letting $t_0 \rightarrow -\infty$, and also eliminate memory effects in the scatterings by Markov approximation in the time integral. In doing this, we assume that Y(t) varies slowly as compared to the exponential factor in the integrand. With this we obtain

$$\mathrm{S}(\mathrm{t})=\left(\frac{\mathcal{P}}{\mathrm{i}\omega}+\pi\delta(\omega)\right)\mathrm{Y}(\mathrm{t})=\pi\mathcal{D}(\omega)\mathrm{Y}(\mathrm{t}), \tag{42}$$

where $\mathcal{P}$ denotes principal value and

$$\mathcal{D}(\omega)\equiv\frac{1}{\mathrm{i}\pi}\frac{\mathcal{P}}{\omega}+\delta(\omega). \tag{43}$$

The Markov approximation here relies on the assumption of different time scales relevant for the interaction-induced correlations on one hand, and the dynamics of distribution functions and polarization on the other hand, and results in a semiclassical approach to the relaxation and dephasing processes. The limitations of this approximation for the carrier-phonon kinetics on a femtosecond scale are discussed in reference 1.

Collecting all the terms and using $\gamma^{e}_{q} = -\gamma^{h}_{q} = \gamma_q$ for interaction with polar phonons, we obtain (*9*)

$$\left.\frac{df^{e}_{\mathbf{k}}}{dt}\right|^{(2)}_{cph} = -\sum_{q}\left[W^{e,cph}_{\mathbf{k-q},\mathbf{k}} f^{e}_{\mathbf{k}} - W^{e,cph}_{\mathbf{k},\mathbf{k-q}} f^{e}_{\mathbf{k-q}}\right] + \frac{1}{i\hbar}\left[F^{e,cph}_{\mathbf{k}} p^{*}_{\mathbf{k}} - F^{e,cph*}_{\mathbf{k}} p_{\mathbf{k}}\right] \tag{44}$$

$$\left.\frac{df^{h}_{\mathbf{k}}}{dt}\right|^{(2)}_{cph} = -\sum_{q}\left[\, W^{h,cph}_{\mathbf{k-q},\mathbf{k}} f^{e}_{k} - W^{h,cph}_{\mathbf{k},\mathbf{k-q}} f^{h}_{\mathbf{k-q}}\right] + \frac{1}{i\hbar}\left[F^{h,cph}_{-\mathbf{k}} p^{*}_{-\mathbf{k}} - F^{h,cph*}_{-\mathbf{k}} p_{-\mathbf{k}}\right] \tag{45}$$

$$\left.\frac{dp_{\mathbf{k}}}{dt}\right|^{(2)}_{cph} = -\sum_{q}\left[W^{p,cph}_{\mathbf{k-q},\mathbf{k}} p_{\mathbf{k}} - W^{p,cph}_{\mathbf{k},\mathbf{k-q}} p_{\mathbf{k-q}}\right], \tag{46}$$

where the internal polarization fields $F^{\alpha,cph}$ are given by

$$F^{\alpha,cph}_{\mathbf{k}} = i\pi \sum_{q} |\gamma_q|^2 \sum_{\pm} (\pm p_{\mathbf{k-q}}) \mathcal{P}\left(\varepsilon^{\alpha}_{\mathbf{k}} - \varepsilon^{\alpha}_{\mathbf{k-q}} \pm \hbar\omega_{\mathbf{q}}\right), \tag{47}$$

the carrier-phonon scattering rates are given by

$$W^{\alpha,cph}_{k-\mathbf{q},\mathbf{k}} = \frac{2\pi}{\hbar} \sum_{\pm -} |\gamma_q|^2 \delta\left(\varepsilon^{\alpha}_{k} - \varepsilon^{\alpha}_{k-q} \pm \hbar\omega_{\mathbf{q}}\right)\left(N_q + \frac{1}{2} \pm \frac{1}{2}\right)\left(1 - f^{\alpha}_{\mathbf{k-q}}\right), \tag{48}$$

and the polarization transition matrices are given by

$$W^{p,cph}_{\mathbf{k-q},\mathbf{k}} = \frac{\pi}{\hbar} \sum_{\alpha=e,h} \sum_{\pm -} |\gamma_q|^2 \mathcal{D}\left(\varepsilon^{\alpha}_{\mathbf{k}} - \varepsilon^{\alpha}_{\mathbf{k-q}} \pm \hbar\omega_{\mathbf{q}}\right)\left[\left(N_q + \frac{1}{2} \mp \frac{1}{2}\right) f^{\alpha}_{\mathbf{k-q}} + \left(N_q + \frac{1}{2} \pm \frac{1}{2}\right)\left(1 - f^{\alpha}_{\mathbf{k-q}}\right)\right] \tag{49}$$

The δ-function part of $\mathcal{D}$ produces the scattering and dephasing terms, while the principal value part produces energy renormalization terms describing polaron corrections to the band structure. It follows from the last two equations that in the low excitation regime, $f^{\alpha} << 1$,

$$W^{p,cph}_{\mathbf{k-q},\mathbf{k}} \approx \frac{1}{2}\sum_{\alpha} W^{\alpha,cph}_{\mathbf{k-q},\mathbf{k}} \tag{50}$$

4.3 Carrier-carrier Interaction

The contributions of carrier-carrier interaction are obtained using the Heisenberg equations of motion. The derivation employs the anti-commutation relations for the electron and hole operators, from which we also derive the following commutation relations:

$$\left[c^+_{k'}c_{k'}, c^+_k\right] = \delta_{k,k'}c^+_k\,, \quad \left[c^+_{k'}c_{k'}, c_k\right] = -\delta_{k,k'}c_k\,, \quad \left[c^+_{k'}d^+_{-k'}, c_k\right] = -\delta_{k,k'}d^+_{-k}\,, \left[c^+_{k'}d^+_{-k'}, c^+_k\right] = 0\,.$$

The resulting c-c contribution to the equation for electron distribution function is given by

$$\left.\frac{df^e_k}{dt}\right|_{cc} = \frac{1}{i\hbar}\sum_{k',q} V_q\left[\left\langle c^+_k c^+_{k'}c_{k'+q}c_{k-q}\right\rangle - \left\langle c^+_{k-q}c^+_{k'+q}c_{k'}c_k\right\rangle - \left\langle c^+_k d^+_{-k'-q}d_{-k'}c_{k-q}\right\rangle + \left\langle c^+_{k-q}d^+_{-k'}d_{-k'-q}c_k\right\rangle\right], \tag{51}$$

and similarly for f^h_k and p_k. The lowest order approximation, the first order contribution, is obtained by factorizing the expectation values of four-operator products into distribution functions and polarization. The results are the Hartree-Fock terms:

$$\left.\frac{df^e_k}{dt}\right|^{(1)}_{cc} = \left.\frac{df^h_{-k}}{dt}\right|^{(1)}_{cc} = \frac{1}{i\hbar}\left(F^{cc(1)}_k p^*_k - F^{cc(1)*}_k p_k\right) \tag{52}$$

$$\left.\frac{dp_k}{dt}\right|^{(1)}_{cc} = \frac{1}{i\hbar}\left[\Sigma_k p_k + F^{cc(1)}_k\left(1 - f^e_k - f^h_{-k}\right)\right], \tag{53}$$

where Σ is the self-energy due to the e-e and h-h interactions, and F is the internal field due to the e-h interaction (interband polarization field):

$$\Sigma_{\mathbf{k}} = -\sum_{k'} V_{\mathbf{k}-\mathbf{k}'}\left(f^e_{\mathbf{k}'} + f^h_{-\mathbf{k}'}\right) \tag{54}$$

$$F^{cc(1)}_k = -\sum_{k'} V_{\mathbf{k}-\mathbf{k}'}p_{k'}\,. \tag{55}$$

The self-energy in equation 54 is a real quantity that renormalizes the one-particle carrier energies $\varepsilon_\alpha(\mathbf{k})$ and does not contribute to a finite lifetime. The effect of the internal field $F^{cc(1)}_{\mathbf{k}}$ is to renormalize the Rabi frequency (*3*), and it can be included in the generation rate:

$$g_k(t) = g^{(0)}_k(t) + g^{(1)}_k(t) = \frac{1}{i\hbar}\left\{\left[M_k E(t)e^{-i\omega_p t} + F^{cc(1)}_k\right]p^*_k - \left[M^*_k E(t)e^{i\omega_p t} + F^{cc(1)*}_k\right]p_k\right\}. \tag{56}$$

The contribution due to the internal field satisfies the sum rule

$$\sum_k g^{(1)}_k = 0 \tag{57}$$

and does not contribute to the generating of electron-hole pairs. It changes the distribution of carriers inside their respective bands, but in contrast to true scattering processes, it is a coherent process (*8*). This renormalization adds nonlinear terms to the evolution equations, which can be used as a mathematical model to study optical nonlinearities in semiconductors (*3*). The scattering processes appear in the second-order contributions. These are obtained from the Heisenberg equations of motion for the two-particle correlations:

$$\delta\langle c_k^+ c_{k'}^+ c_{k'+q} c_{k-q}\rangle = \langle c_k^+ c_{k'}^+ c_{k'+q} c_{k-q}\rangle + f_k^e f_{k'}^e \delta_{k',k-q} \tag{58}$$

$$\delta\langle c_k^+ d_{-k'-q}^+ d_{-k'} c_{k-q}\rangle = \langle c_k^+ d_{-k'-q}^+ d_{-k'} c_{k-q}\rangle - p_k^* p_{k'} \delta_{k',k-q},$$

which describe deviations from the corresponding factorizations.

The resulting equations for these two-particle correlation functions contain three-particle correlations, which are factorized into two-particle correlations, distribution functions, and polarizations (*9*). If the two-particle correlations are further factorized into distribution functions, the resulting equation for the correlation function in equation 58 is given by

$$i\hbar \frac{d}{dt}\,\delta\langle c_k^+ c_{k'}^+ c_{k'+q} c_{k-q}\rangle = [-\varepsilon_e(k) - \varepsilon_e(k') + \varepsilon_e(k'+q) + \varepsilon_e(k-q)]\delta\langle c_k^+ c_{k'}^+ c_{k'+q} c_{k-q}\rangle \tag{59}$$

$$+\left(V_q - V_{k-k''-q}\right)\left[f_k^e f_{k'}^e\left(1 - f_{k'+q}^e\right)\left(1 - f_{k-q}^e\right) - f_{k-q}^e f_{k'+q}^e\left(1 - f_{k'}^e\right)\left(1 - f_k^e\right)\right]$$
$$+ V_q\left[p_{k-q} p_k^*\left(f_{k'+q}^e - f_{k'}^e\right) + p_{k'+q} p_{k'}^*\left(f_{k-q}^e - f_k^e\right)\right]$$
$$- V_{k-k'-q}\left[p_{k-q} p_{k'}^*\left(f_{k'+q}^e - f_k^e\right) + p_{k'+q} p_k^*\left(f_{k-q}^e - f_{k'}^e\right)\right] .$$

This equation is of the same form as equation 40 for carrier-phonon correlation function S^e. We transform it into the integral equation as in equation 41 and perform adiabatic and Markov approximations. The result is then used in equation 51 to obtain the second-order c-c interaction terms in the kinetic equation for electron distribution function. Have we retained the two-particle correlations in equation 59, the bare Coulomb interaction $V_q^{(0)} = e^2/(V\varepsilon_0\varepsilon_s q^2)$ in the kinetic equation for $f_{\mathbf{k}}^e$ would become dynamically screened with the Lindhard dielectric function of electron gas (*1, 16*):

$$V_{\mathbf{q}}^{(0)} \rightarrow \frac{V_q^{(0)}}{\epsilon\left[\mathbf{q}, \left(\varepsilon_{\mathbf{k}-\mathbf{q}}^e - \varepsilon_{\mathbf{k}}^e\right)/\hbar\right]} \tag{60}$$

where

$$\epsilon(\mathbf{q}, \omega) = 1 - V_{\mathbf{q}}^{(0)} \sum_{\mathbf{k}} \frac{f_{\mathbf{k}}^e - f_{\mathbf{k}-\mathbf{q}}^e}{\varepsilon_k^e - \varepsilon_{\mathbf{k}-\mathbf{q}}^e - \hbar\omega} \ . \tag{61}$$

In this work we use the static limit of equation 61, and for V_q in kinetic equations, we use Coulomb interaction statically screened by electrons and holes, thus obtaining the screened

Coulomb interaction in equation 7 with the inverse screening length given in equation 8. The dynamic screening effects that would lead to carrier-plasmon scattering, are excluded in this approximation. With these approximations, the carrier-carrier interaction second-order terms in the kinetic equations are the following:

$$\left.\frac{df_{\mathbf{k}}^{e}}{dt}\right|_{cc}^{(2)} = -\sum_{q}\left[W_{\mathbf{k}-\mathbf{q},\mathbf{k}}^{e,cc} f_{\mathbf{k}}^{e} - W_{\mathbf{k},\mathbf{k}-\mathbf{q}}^{e,cc} f_{\mathbf{k}-\mathbf{q}}^{e}\right] + \frac{1}{i\hbar}\left[F_{\mathbf{k}}^{e,cc} p_{\mathbf{k}}^{*} - F_{\mathbf{k}}^{e,cc*} p_{\mathbf{k}}\right] \tag{62}$$

$$\left.\frac{df_{\mathbf{k}}^{h}}{dt}\right|_{cc}^{(2)} = -\sum_{q}\left[\, W_{\mathbf{k}-\mathbf{q},\mathbf{k}}^{h,cc} f_{k}^{e} - W_{\mathbf{k},\mathbf{k}-\mathbf{q}}^{h,cc} f_{\mathbf{k}-\mathbf{q}}^{h}\right] + \frac{1}{i\hbar}\left[F_{-\mathbf{k}}^{h,cc(2)} p_{-\mathbf{k}}^{*} - F_{-\mathbf{k}}^{h,cc(2)*} p_{-\mathbf{k}}\right] \tag{63}$$

$$\left.\frac{dp_{\mathbf{k}}}{dt}\right|_{cc}^{(2)} = -\sum_{q}\left[W_{\mathbf{k}-\mathbf{q},\mathbf{k}}^{p,cc} p_{\mathbf{k}} - W_{\mathbf{k},\mathbf{k}-\mathbf{q}}^{p,cc} p_{\mathbf{k}-\mathbf{q}}\right], \tag{64}$$

where the internal polarization fields $F^{\alpha,cc(2)}$ are given by

$$F_{\mathbf{k}}^{\alpha,cc(2)} = i\pi \sum_{\mathbf{k}',q} |V_q|^2 \sum_{\alpha'} \left(f_{\mathbf{k}'+\mathbf{q}}^{\alpha'} - f_{\mathbf{k}'}^{\alpha'}\right) p_{\mathbf{k}-\mathbf{q}} \mathcal{D}\left(\varepsilon_{\mathbf{k}}^{\alpha} - \varepsilon_{\mathbf{k}-\mathbf{q}}^{\alpha} + \varepsilon_{\mathbf{k}'}^{\alpha'} - \varepsilon_{\mathbf{k}'+\mathbf{q}}^{\alpha'}\right), \tag{65}$$

the carrier-carrier transition matrices are given by

$$W_{k-\mathbf{q},\mathbf{k}}^{\alpha,cc} = \frac{\pi}{\hbar}|V_q|^2 \sum_{\alpha'}\sum_{k'} \mathcal{D}\left(\varepsilon_{k-q}^{\alpha} - \varepsilon_{k}^{\alpha} + \varepsilon_{k'+q}^{\alpha'} - \varepsilon_{k'}^{\alpha'}\right)\left(1 - f_{\mathbf{k}-\mathbf{q}}^{\alpha}\right)\left[f_{k'}^{\alpha'}\left(1 - f_{k'+q}^{\alpha'}\right) - p_{k'+q}^{*} p_{k'}\right] + \text{c.c.}, \tag{66}$$

and the polarization transition matrices are given by

$$W_{\mathbf{k}-\mathbf{q},\mathbf{k}}^{p,cc} = \frac{\pi}{\hbar}|V_q|^2 \sum_{\alpha,\alpha'}\sum_{k'} \mathcal{D}\left(\varepsilon_{\mathbf{k}-\mathbf{q}}^{\alpha} - \varepsilon_{\mathbf{k}}^{\alpha} + \varepsilon_{\mathbf{k}'+\mathbf{q}}^{\alpha'} - \varepsilon_{k'}^{\alpha'}\right)\left[-p_{\mathbf{k}'+\mathbf{q}}^{*} p_{k'} + f_{k'}^{\alpha'}\left(1 - f_{\mathbf{k}'+\mathbf{q}}^{\alpha'}\right)\left(1 - f_{\mathbf{k}-\mathbf{q}}^{\alpha}\right) + f_{\mathbf{k}-\mathbf{q}}^{\alpha} f_{\mathbf{k}'+\mathbf{q}}^{\alpha'}\left(1 - f_{\mathbf{k}'}^{\alpha'}\right)\right]. \tag{67}$$

4.4 Kinetic Equations to the Second-order in Carrier-phonon and Carrier-carrier Interactions

With the interaction terms derived in section 4.3, the equations of motion can be written as

$$\frac{df_{\mathbf{k}}^{\alpha}}{dt} = g_{\mathbf{k}}^{\alpha}(t) - \sum_{\mathbf{q}}\left[W_{\mathbf{k}-\mathbf{q},\mathbf{k}}^{\alpha} f_{k}^{\alpha} - W_{\mathbf{k},\mathbf{k}-\mathbf{q}}^{\alpha} f_{\mathbf{k}-\mathbf{q}}^{\alpha}\right] \tag{68}$$

$$\frac{\mathrm{dp_{\mathbf{k}}}}{\mathrm{dt}} = \frac{1}{i\hbar}(\mathcal{E}^{\mathrm{e}}_{\mathrm{k}} + \mathcal{E}^{\mathrm{e}}_{-\mathrm{k}})\mathrm{p_{\mathbf{k}}} + \frac{1}{\mathrm{i}\hbar}\mathcal{F}^{\mathrm{p}}_{\mathrm{k}}(\mathrm{t})\left(1 - \mathrm{f}^{\mathrm{e}}_{\mathrm{k}} - \mathrm{f}^{\mathrm{h}}_{\mathrm{k}}\right) - \sum_{\mathbf{q}}\left[\mathrm{W}^{\mathrm{p}}_{\mathbf{k-q},\mathbf{k}}\mathrm{p_{\mathbf{k}}} - \mathrm{W}^{\mathrm{p}}_{\mathbf{k},\mathbf{k-q}}\mathrm{p_{\mathbf{k-q}}}\right], \tag{69}$$

with the renormalized energies of carriers (Hartree-Fock terms)

$$\mathcal{E}^{\mathrm{e}}_{\mathrm{k}} = \varepsilon^{\alpha}_{k} + \Sigma_{k}, \tag{70}$$

the fields given by the sum of the applied field the and internal polarization fields

$$\mathcal{F}^{\alpha}_{\mathrm{k}} = \mathrm{M_k E(t)e^{-i\omega_p t}} + \mathrm{F}^{\alpha,\mathrm{cph}}_{\mathrm{k}} + \mathrm{F}^{\alpha,\mathrm{cc(1)}}_{\mathrm{k}} + \mathrm{F}^{\alpha,\mathrm{cc(2)}}_{\mathrm{k}} \tag{71}$$

$$\mathcal{F}^{\mathrm{p}}_{\mathrm{k}} = \mathrm{M_k E(t)e^{-i\omega_p t}} + \mathrm{F}^{\alpha,\mathrm{cc(1)}}_{\mathrm{k}}, \tag{72}$$

the generation rate

$$\mathrm{g}^{\alpha}_{\mathrm{k}}(\mathrm{t}) = \frac{1}{i\hbar}[\mathcal{F}^{\alpha}_{\mathrm{k}}\mathrm{p}^{*}_{\mathrm{k}} - \mathcal{F}^{\alpha *}_{\mathrm{k}}\mathrm{p_k}], \tag{73}$$

and with transition matrices $\mathrm{W}^{\alpha}_{\mathbf{k},\mathbf{k-q}}$ and $\mathrm{W}^{\mathrm{p}}_{\mathbf{k},\mathbf{k-q}}$ being the sums of the second-order carrier-phonon and carrier-carrier interaction transition matrices. The transition matrices $\mathrm{W}^{\alpha}_{\mathbf{k},\mathbf{k-q}}$ (α = e, h) for the distribution functions are real quantities but are not necessarily positive. The transition matrix for the polarization $\mathrm{W}^{\mathrm{p}}_{\mathbf{k},\mathbf{k-q}}$ is a complex quantity. Its real part describes scattering processes that contribute to the dephasing of polarization, and the imaginary part describes second-order contributions to the band gap renormalization. The second-order energy shifts are usually negligible as compared to the Hartree-Fock energy renormalization (*1*).

4.5 Luminescence Spectrum

In this work, we will not consider the emission of coherent photons possible in the presence of coherent interband polarization (*8*), and the luminescence spectrum will be evaluated from the Fermi Golden Rule. It results from evaluation of the rate of emitted photons using Markov approximation of the carrier-photon interaction in the luminescence to the second-order. With the carrier-carrier distribution functions obtained from the kinetic equations 68 and 69, and the momentum of emitted photons approximated by zero, the luminescence spectrum is given by

$$\mathrm{I_{em}}(\omega) = \frac{2\pi}{\hbar}\sum_{\mathrm{k}}\mathrm{d}^{2}_{\mathrm{cv}}\,\delta\left(\varepsilon^{\mathrm{e}}_{\mathrm{k}} + \varepsilon^{\mathrm{h}}_{-\mathrm{k}} - \hbar\omega\right)\mathrm{f}^{\mathrm{e}}_{\mathrm{k}}\mathrm{f}^{\mathrm{h}}_{\mathrm{k}}\,. \tag{74}$$

Thus, the luminescence spectrum is proportional to the product of electron and hole distribution functions multiplied by the joint density of states. The numerical solutions obtained using a generalized Monte Carlo simulation (*8, 9*) will be shown in section 7.

5. Relaxation Time Approximation

A relaxation time approximation of collision terms in kinetic equations allows use of a simple model to study coherent effects related to optical interband transitions. In this model, different momentum values decouple, and one ends with effectively a two-level system whose dynamics can be described by evolution of a three component Bloch vector (*3*). Define the components as follows:

$$\begin{aligned} U_{1k}(t) &\equiv e^{-i\omega_p t} p_k^*(t) + e^{i\omega_p t} p_k(t) \\ U_{2k}(t) &\equiv -i\left(e^{-i\omega_p t} p_k^*(t) - e^{i\omega_p t} p_k(t) \right) \\ U_{3k} &\equiv 1 - f_k^e(t) - f_k^h(t), \end{aligned} \tag{75}$$

and define detuning by equation 26: $\hbar\Delta_k = \varepsilon_k^e + \varepsilon_k^h - \hbar\omega_p$. Then from equations 23–25, and allowing for relaxation, the optical Bloch equations are

$$\begin{aligned} \frac{dU_{1k}}{dt} &= -\Delta_k U_{2k} - \frac{U_{1k}}{T_{2k}} \\ \frac{dU_{2k}}{dt} &= \Delta_k U_{1k} + 2\Omega_R^{(0)} E(t) U_{3k} - \frac{U_{2k}}{T_{2k}} \\ \frac{dU_{3k}}{dt} &= -2\Omega_R^{(0)} E(t) U_{2k} - \frac{1 - U_{3k}}{T_{1k}}, \end{aligned} \tag{76}$$

with the initial conditions

$$U_{3k}(-\infty) = 1, \quad U_{1k}(-\infty) = U_{2k}(-\infty) = 0. \tag{77}$$

The equations without relaxation describe a rotation of vector $\mathbf{U}_k$ about vector $\mathbf{\Omega} = [-2\Omega_R{}^{(0)}E(t), 0, \Delta_k]$, in which case they can be written as one vector equation: $d\mathbf{U}/dt = \mathbf{\Omega} \times \mathbf{U}$. In view of the discussion in section 3, we assume that the relaxation in this model is due to carrier-phonon interaction, and we set the population decay time T_1 ("longitudinal relaxation time") to be given by the inverse of the sum of electron-phonon and hole-phonon rates:

$$T_{1k} = \frac{1}{\Gamma_k^{e-ph} + \Gamma_k^{h-ph}}. \tag{78}$$

In view of the approximation in equation 50, the polarization decay time T_2 ("transverse relaxation time") is twice the population decay time, $T_{2k} = 2T_{1k}$.

In the absence of relaxation, the carrier distribution function obtained from the optical Bloch equations will exhibit time oscillations with the Rabi frequency. If the difference between the pulse central frequency and the band gap is appreciatively smaller than the LO polar phonon frequency, one expects a significantly reduced carrier-phonon relaxation in GaN at room temperature, in which case the Rabi oscillations should be seen in the time-resolved luminescence. The luminescence evaluated in this model at room temperature is shown in figure 7 for three values of excitation energy relative to the band gap, at two different values of excitation power.

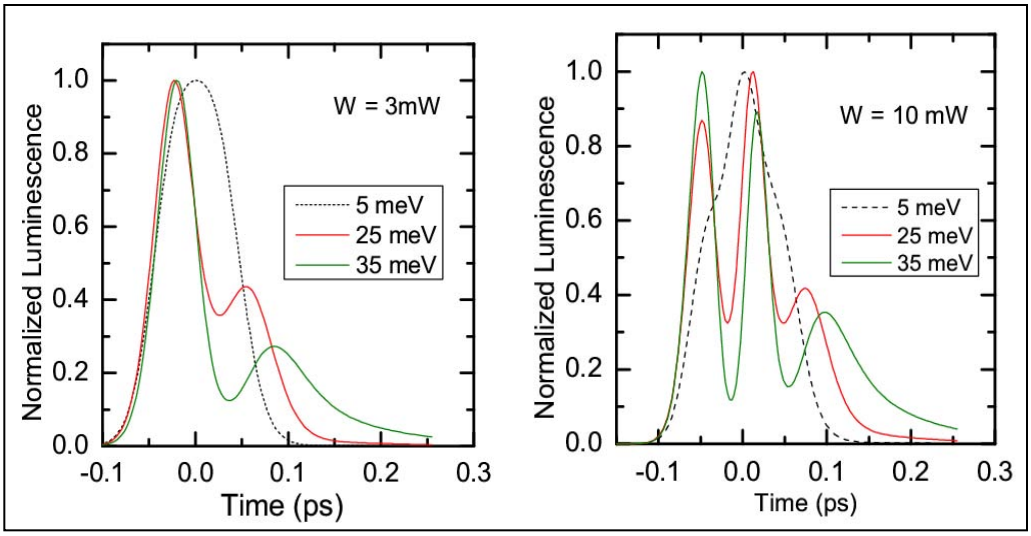

Figure 7. Luminescence evaluated in relaxation model at room temperature for three values of excitation energy relative to the band gap, at two different values of excitation power.

These results indicate a possibility of observing coherent oscillations in the time-resolved luminescence experiments in high quality GaN.

6. Experimental Studies of the Time Resolved Spectroscopy of UV Luminescence

A schematic representation of the experimental setup (*7*) is shown in figure 8. A 250-KHz regeneratively amplified Ti:Sappfire laser produces 150 fs pulses at 800 nm wavelength. Part of this beam is split off, acting as a gating pulse, and the other part pumps an optical parametric amplifier tunable from 720 to 450 nm. Output from the amplifier is again doubled in a nonlinear optical crystal (2Xtal) to produce pulses tunable from 360 to 225 nm. The pump pulse, compressed to a width of approximately 80 fs, is focused onto the sample where it photo-excites electron-hole pairs. The luminescence from the sample is collected using non-dispersive optics and focused on another nonlinear crystal (NLXtal), where it is mixed with the gating pulse to yield a down-converted signal at lower frequency (visible light) that is spatially separated from

the other beam. The down-converted signal is passed through a spectrometer and detected with a photomultiplier tube in photon counting mode. The sample used in these experiments was a 1 μm thick homoepitaxial GaN film deposited on a GaN substrate. The arrival time of the gate pulse relative to the photoluminescence is used to follow the temporal evolution of UV photoluminescence with 350 fs resolution.

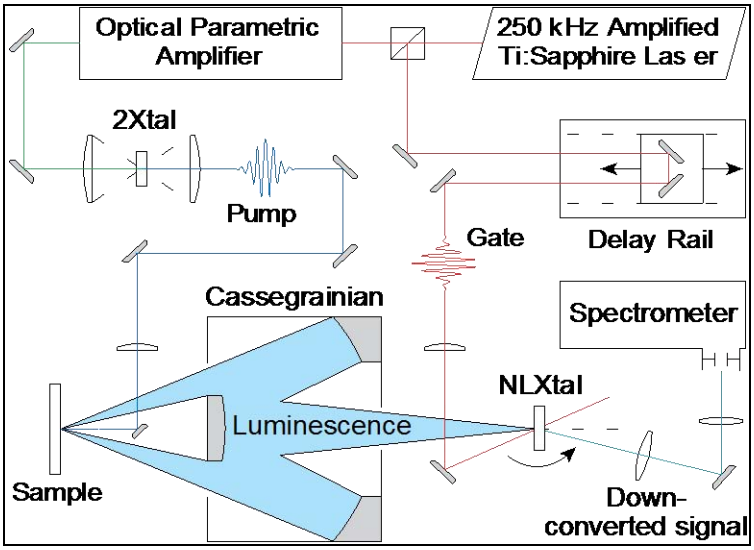

Figure 8. A schematic representation of the setup for the time-resolved photoluminescence experiment. A Ti:Sapphire laser produces 150 fs, 5 mJ, 800 nm pulses. Part of the beam pumps an optical parametric amplifier tunable from 720 to 450 nm. An up-converted beam with pulses tunable from 360 to 225 nm and widths of 50 to 80 fs, pumps energy from 3.44 to 5.5 eV, suitable for studying nitride materials, generates electron-hole pairs in a GaN sample.

The experiments were performed at two values of pump pulse power, 0.66 mW and 2 mW, generating about 8×10^{18} and 2.5×10^{19} electron-hole pairs, respectively. In the experiments, the luminescence was measured at a fixed energy, thus allowing us to watch the carrier distribution pass through a spectral window, as shown in figure 9.

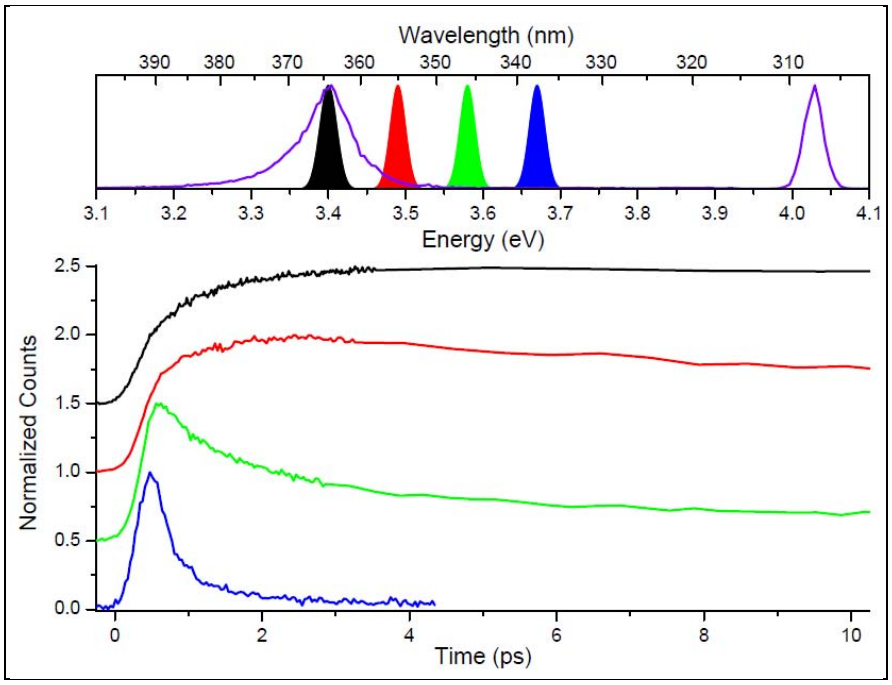

Figure 9. The upper part illustrates the energy position of 2 mW pump pulse, at 308 nm wavelength, and four different values of emission energy. The band edge exciton luminescence lineshape is also shown. The lower part shows the time dependence of the measured photoluminescence at those values of emission energy, set near the band edge (black), $\hbar\omega_{LO}$ (red), 2 $\hbar\omega_{LO}$ (green), and $3\hbar\omega_{LO}$ (blue), where $\hbar\omega_{LO}$ referes to the energy of a polar longitudinal phonon, 91.2 meV.

Room temperature time-resolved photoluminescence obtained with a 308 nm pump (about 75 meV above the conduction band edge) is also shown in figure 10 for two values of the excitation power, 0.66 mW and 2 mW.

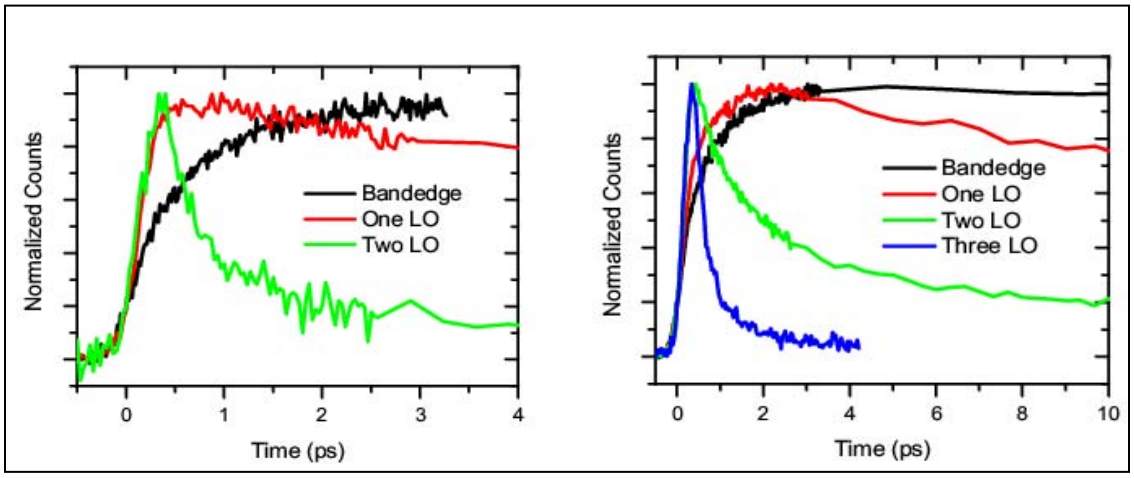

Figure 10. Time evolution of photo-luminescence from GaN at different wavelengths. The pump wavelength is 308 nm, at two values of the pump power, 0.66 mW (left panel) and 2 mW (right panel).

The data are indicative of the rapid formation of a non-thermal distribution associated with the interplay of carrier-carrier scattering (electron-electron and hole-hole) and electron-LO phonon scattering during carrier injection. After injection, a measurable rise time to peak emission is present and is a function of excitation energy, carrier density, and emission energy. Since the time-resolved signal at a given wavelength is proportional to the product of the electron and hole distribution functions at a given momentum, these plots provide a measure of the evolution of the carrier distributions as they cool down to the band edge and into possible deeper band tail states.

Carrier density-dependent data, shown in figure 11, shows the effects of screening in evolution of electron-hole distribution. For an initial excess energy of 0.75 eV (308 nm excitation pulse), a shift of the 355.6 nm (1LO phonon energy above the conduction band edge) emission peak from 0.9 ps to 2.2 ps is seen for a change in density from 8×10^{18} to 2.5×10^{19} cm^{-3} (660 µW to 2 mW pump). The fact that the emission peak is reached later at this wavelength at higher carrier density implies that the electrons relax more slowly due to more efficient screening of the electron-LO phonon interaction.

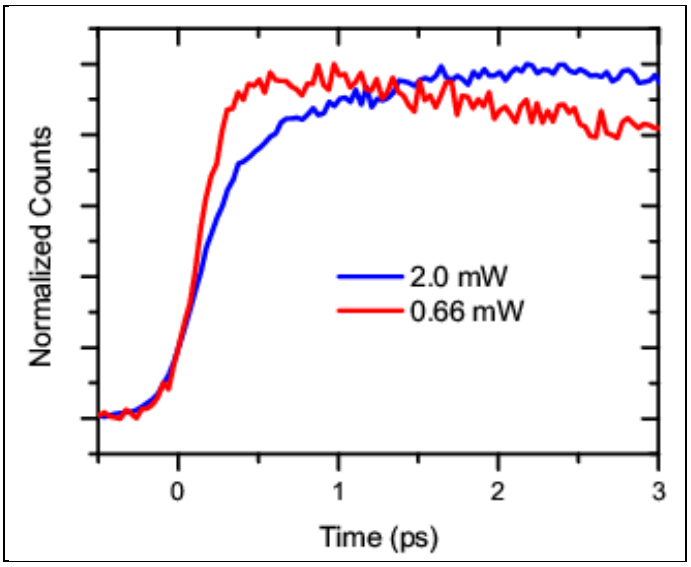

Figure 11. Pump power dependence of 355.6 nm emission showing an increase in rise time at higher density due to screening of the electron-LO phonon interaction.

These experiments allowed us to study initial thermalization and hot carrier dynamics in photo-excited GaN. Screening effects were observed as a function of excitation intensity, and a dependence on the excitation photon energy is seen in the dynamics of the photo-excited carrier distributions.

7. Monte Carlo Simulation of Kinetic Equations

The numerical method we used in the simulation is the Monte Carlo method generalized by Kuhn and Rossi to account for the effects of the interband polarization (*8*). The various contributions to the carrier dynamics in equations 68 and 69 can be separated into two parts, the coherent part and dephasing part. Let $\mathcal{R}_k^\nu$ be a kinetic variable, being $f_k^{e,h}$ if ν = e,h or p_k if ν = p. The kinetic equations can be schematically written as

$$\frac{\mathrm{d}}{\mathrm{dt}}\mathcal{R}_{\mathrm{k}}^{\nu} = \frac{\mathrm{d}}{\mathrm{dt}}\mathcal{R}_{\mathrm{k}}^{\nu}\Big|_{\mathrm{coher}} + \frac{\mathrm{d}}{\mathrm{dt}}\mathcal{R}_{\mathrm{k}}^{\nu}\Big|_{\mathrm{incoh}}, \quad \nu = \mathrm{e,h,p} \tag{79}$$

with

$$\frac{\mathrm{d}}{\mathrm{dt}}\mathcal{R}_{\mathrm{k}}^{\nu}\Big|_{\mathrm{coher}} = \mathcal{G}_{\mathrm{k}}^{\nu,0}(\{\mathcal{R}^{\nu}\}) + \sum_{\mathrm{j}\neq 0}\mathcal{G}_{\mathrm{k}}^{\nu,\mathrm{j}}(\{\mathcal{R}^{\nu}\}) \tag{80}$$

$$\frac{\mathrm{d}}{\mathrm{dt}}\mathcal{R}_{\mathrm{k}}^{\nu}\Big|_{\mathrm{incoh}} = \sum_{\mathrm{j,k'}}\left[\mathcal{W}_{\mathrm{k,k'}}^{\nu,\mathrm{j}}\mathcal{R}_{\mathrm{k'}}^{\nu} - \mathcal{W}_{\mathrm{k',k}}^{\nu,\mathrm{j}}\mathcal{R}_{\mathrm{k}}^{\nu}\right],$$

where $\mathcal{G}_{\mathrm{k}}^{\nu,\mathrm{j}}$ is a functional of kinetic variables, and $\mathcal{W}_{\mathrm{k,k'}}^{\nu,\mathrm{j}}$ is the scattering rate associated with kinetic variable $\mathcal{R}^{\nu}$ for a transition $\mathbf{k} \rightarrow \mathbf{k'}$ induced by the jth interaction mechanism. These rates are real positive quantities, unlike the full transition matrices $\mathrm{W}_{\mathrm{k,k'}}^{\nu,\mathrm{j}}$.

The coherent part describes the generation of carriers and polarization, which are highly correlated due to the external field. This part is evaluated by a direct numerical integration. Under the approximations used in the derivation of kinetic equations in this work, the incoherent part has basically the same form as used in traditional Monte Carlo simulation. The only difference is that the polarization is a complex quantity.

The total time is divided into time steps, Δt, and the system is initialized in vacuum state at t_0. In this state, the distribution functions and the polarization are zero. For each step, we compute the coherent part by the direct integration. In the Monte Carlo "sampling" of incoherent contributions for each kinetic variable $\mathcal{R}^{\nu}$, we use an ensemble of N particles generated randomly according to the distribution function $|\mathcal{R}^{\nu}|$. For the polarization, a phase is attached according to the phase of p_k. The traditional Monte Carlo simulation is performed according to the scattering rates $\mathcal{W}_{\mathrm{k,k'}}^{\nu,\mathrm{j}}$. A more detailed description can be found in reference 9. The conduction band nonparabolicity and static screening were included in the calculations. Once the distribution functions are obtained, the luminescence is evaluated from equation 74. The results in figure 12 show that the rise of the experimentally observed luminescence and the associated rise-times are in reasonable agreement with experimental results in section 6, confirming that the

carrier-polar optical phonon interaction is the dominant scattering mechanism in the subpicosecond evolution of photo-excited carriers.

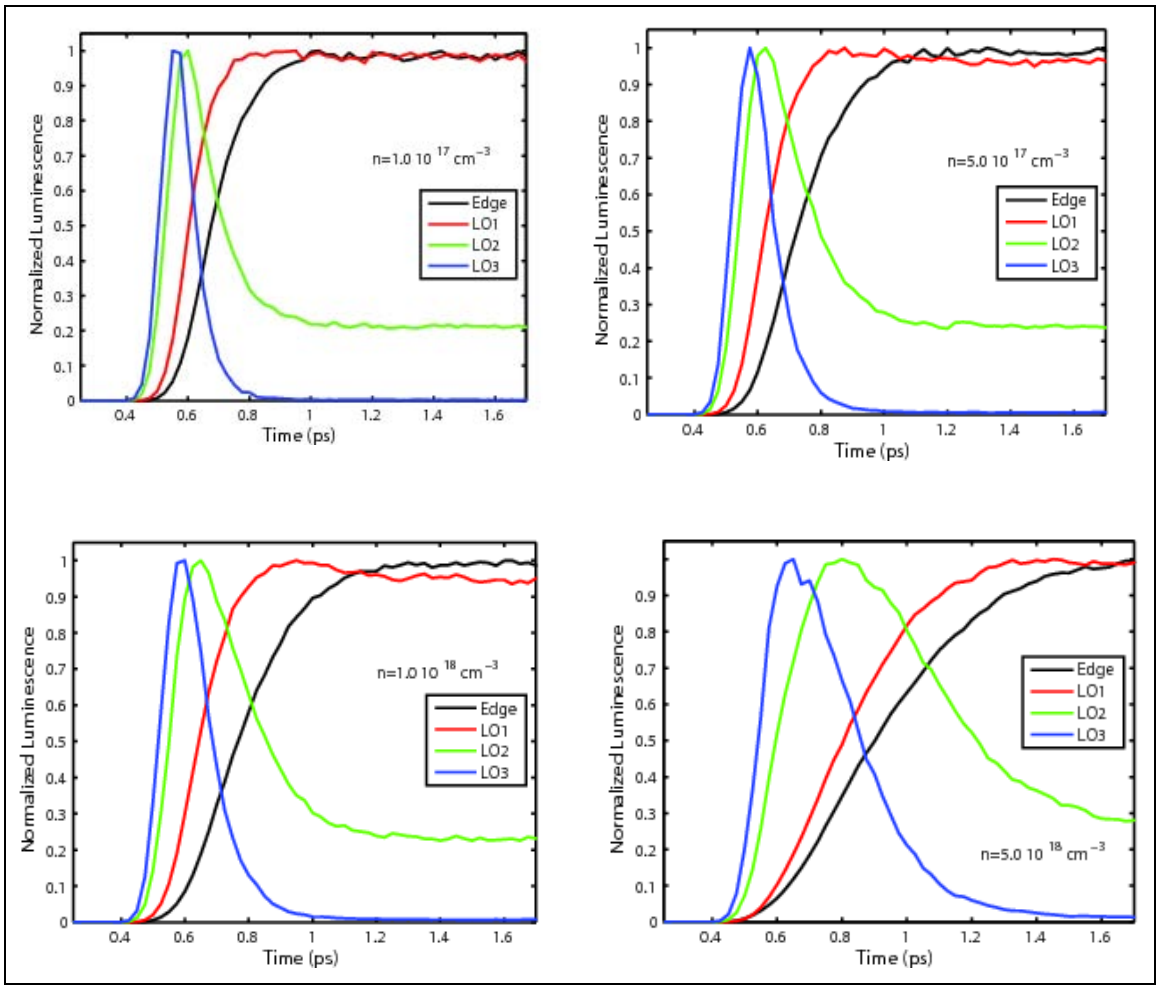

Figure 12. Theoretical luminescence from photo-excited GaN obtained by Monte Carlo simulation of kinetics equations. Luminescence is shown as function of time at four different energies, at the band edge and at one, two, and three times LO-phonon energy above the band gap.

8. Conclusions

We have applied the SBE formalism to study the subpicosecond dynamics of photo-excited carriers in GaN. The kinetics equations were derived using a two-band model and taking into account the coherent interaction of semiconductor with the short laser pulse. Various scattering terms due to interaction of carriers with polar optical phonons and carrier-carrier interaction were taken into account. Effects of the conduction band nonparabolicity and static screening were included in our theory. Prior to the evaluation of kinetics, we calculated scattering rates and

found that the relaxation of carriers in bulk GaN is dominated by electron-polar phonon scattering, with rates much higher than the corresponding rates in GaAs, for example. We also found that the plasmon emission by energetic electrons can be a substantial contributing mechanism to the hot electron relaxation on the subpicosecond scale, though not nearly as important as carrier-optical phonon scattering. Further investigation of possible plasmon effects may be included in the future theoretical work on hot carrier dynamics in GaN. This will involve using dynamic carrier screening rather than the static approximation. We find reasonable agreement with the experimental results on the time-resolved photoluminescence rise-time dependence on excitation energy and carrier density, thus confirming the dominant role of polar optical phonons in the subpicosecond dynamics, and the effects of screening. The results of the relaxation model suggest a possibility of observing coherent polarization effects, the Rabi oscillations in luminescence, possibly using different wide-band-gap polar material samples at lower pump power. An extension of the experiments to lower temperatures would also be of interest to further clarify the role of polar phonons in subpicosecond hot electron dynamics.

9. References

1. Rossi, F.; Kuhn, T. *Rev. Mod. Phys*. **2002**, *74*, 895.
2. Jacoboni, L.; Lugli, P. The *Monte Carlo Method for Semiconductor Device Simulation*; Springer-Verlag, New York, 1989.
3. Haug, H; Koch, S. W. *Quantum Theory of the Optical and Electronic Properties of Semiconductors*; 3d edition 1994, World Scientific.
4. Ridley, B. K. *Quantum Processes in Semiconductors*; 4th edition 1999, Clarendon Press, Oxford.
5. Conwell, E. M.; Vassell, M. O. *Phys. Rev* **1968**, *166*, 797.
6. Wang, Y.; Bellotti, E.; Wraback, M.; Rudin S. *Proceedings of 27th Int. Conf. on the Physics of Semiconductors*, ed. J. Menendez and C. G. Van de Walle, AIP 2005, 239.
7. Garrett, G. A.; Rudin, S.; Sampath, A. V.; Collins, C. J.; Shen, H.; Wraback, M. *Proceedings of 27th Int. Conf. on the Physics of Semiconductors*, ed. J. Menendez and C. G. Van de Walle, AIP 2005, 243.
8. Kuhn, T.; Rossi, F. *Phys. Rev. B* **1992**, *46*, 7496.
9. Haas, S.; Rossi, F.; Kuhn, T. *Phys. Rev. B* **1996**, *53*, 12855.
10. Conwell, E. M.; Vassell, M. O. *Phys. Rev* **1968**, *166*, 797.
11. Goano, M.; Bellotti, E.; Ghillino E.; Ghione G.; Brennan K. F. *J. Appl. Phys*. **2000**, *88*, 6467.
12. Osman, M. A.; Ferry, D. K. *Phys. Rev. B* **1987**, *36*, 6018.
13. Mahan G. D. in *Polarons in Ionic Crystals and Polar Semiconductors*, edited by J. T. Devreese 1972 (North-Holland, Amsterdam), p. 553.
14. Diff, K.; Brennan, K. F. *J. Appl Phys.* **1991**, *69*, 3097.
15. Madelung O. *Introduction to Solid-Stare Theory;* Springer, Heidelberg, 1978.
16. Wyld, H. W.; Fried, B. D. *Ann. Phys. (N. Y.)* **1963**, *23*, 374.

List of Acronyms and Abbreviations

2Xtal	nonlinear optical crystal
AlGaN	aluminum gallium nitride
Fs	femtosecond
GaAs	gallium arsenide
GaN	gallium nitride
LO	longitudinal optical
NLXtal	nonlinear crystal
RPA	Random Phase Approximation
SBE	Semiconductor Bloch Equation
TRPL	time-resolved photoluminescence
UV	ultraviolet

NO. OF COPIES	ORGANIZATION
1 ELEC	ADMNSTR DEFNS TECHL INFO CTR ATTN DTIC OCP 8725 JOHN J KINGMAN RD STE 0944 FT BELVOIR VA 22060-6218
1 CD	OFC OF THE SECY OF DEFNS ATTN ODDRE (R&AT) THE PENTAGON WASHINGTON DC 20301-3080
1	US ARMY RSRCH DEV AND ENGRG CMND ARMAMENT RSRCH DEV & ENGRG CTR ARMAMENT ENGRG & TECHNLGY CTR ATTN AMSRD AAR AEF T J MATTS BLDG 305 ABERDEEN PROVING GROUND MD 21005-5001
1	PM TIMS, PROFILER (MMS-P) AN/TMQ-52 ATTN B GRIFFIES BUILDING 563 FT MONMOUTH NJ 07703
1	US ARMY INFO SYS ENGRG CMND ATTN AMSEL IE TD A RIVERA FT HUACHUCA AZ 85613-5300
1	COMMANDER US ARMY RDECOM ATTN AMSRD AMR W C MCCORKLE 5400 FOWLER RD REDSTONE ARSENAL AL 35898-5000
1	US GOVERNMENT PRINT OFF DEPOSITORY RECEIVING SECTION ATTN MAIL STOP IDAD J TATE 732 NORTH CAPITOL ST NW WASHINGTON DC 20402
1	BOSTON UNIVERSITY ELECTRICAL AND COMPUTER ENGINEERING DEPT ATTN E BELLOTTI 8 SAINT MARY'S ST BOSTON MA 02215-2421

NO. OF COPIES	ORGANIZATION
1	US ARMY RSRCH LAB ATTN RDRL WM S KARNA BLDG 4600 ABERDEEN PROVING GROUND MD 21005
1	US ARMY RSRCH LAB ATTN RDRL CIM G T LANDFRIED BLDG 4600 ABERDEEN PROVING GROUND MD 21005-5066
12	US ARMY RSRCH LAB ATTN IMNE ALC HRR MAIL & RECORDS MGMT ATTN RDRL CIM L TECHL LIB ATTN RDRL CIM P TECHL PUB ATTN RDRL SEE M G GARRETT ATTN RDRL SEE M L STOUT ATTN RDRL SEE M M REED ATTN RDRL SEE M M WRABACK ATTN RDRL SEE M S RUDIN (3 HCS) ATTN RDRL SER A HUNG ATTN RDRL SER E F CROWNE ADELPHI MD 20783-1197

TOTAL: 22 (1 ELECT, 1 CD, 20 HCS)

INTENTIONALLY LEFT BLANK.